



Mathematical Modeling of Tumor-Induced Angiogenesis

M.A.J. Chaplain,¹ S.R. McDougall,² and A.R.A. Anderson¹

¹The SIMBIOS Center, Division of Mathematics, University of Dundee, Dundee DD1 4HN, Scotland;
email: chaplain@maths.dundee.ac.uk, sanderso@maths.dundee.ac.uk

²Institute of Petroleum Engineering, Heriot-Watt University, Edinburgh EH14 4AS, Scotland;
email: Steve.McDougall@pet.hw.ac.uk

Annu. Rev. Biomed. Eng.
2006. 08:11.1–11.25

The *Annual Review of
Biomedical Engineering* is
online at
bioeng.annualreviews.org

doi: 10.1146/
annurev.bioeng.8.061505.095807

Copyright © 2006 by
Annual Reviews. All rights
reserved

1523-9829/06/0815-
0001\$20.00

Key Words

blood vessels, microvasculature, endothelial cell migration,
network flow, drug delivery

Abstract

Angiogenesis, the growth of a network of blood vessels, is a crucial component of solid tumor growth, linking the relatively harmless avascular and the potentially fatal vascular growth phases of the tumor. As a process, angiogenesis is a well-orchestrated sequence of events involving endothelial cell migration and proliferation; degradation of tissue; new capillary vessel formation; loop formation (anastomosis) and, crucially, blood flow through the network. Once there is flow associated with the nascent network, subsequent growth evolves both temporally and spatially in response to the combined effects of angiogenic factors, migratory cues via the extracellular matrix, and perfusion-related hemodynamic forces in a manner that may be described as both adaptive and dynamic. In this article, we first present a review of previous theoretical and computational models of angiogenesis and then indicate how recent developments in flow models are providing insight into antiangiogenic and chemotherapeutic drug treatment of solid tumors.

Angiogenesis: the formation of new blood vessels from a preexisting vasculature

Vasculature: a network of capillary blood vessels

Endothelial cells (ECs): cells lining all the blood vessels and arteries

TAF: tumor angiogenic factor

Angiogenic factors: soluble, diffusible chemicals that stimulate endothelial cells to proliferate and migrate

PDE: partial differential equation

INTRODUCTION

Angiogenesis is the process by which new blood vessels develop from an existing vasculature, through endothelial cell sprouting, proliferation, and fusion (1). Adult endothelial cells are normally quiescent and, apart from certain developmental processes (e.g., embryogenesis) and wound healing, angiogenesis is generally a pathological process implicated in arthritis (2); some eye diseases; and solid tumor development, invasion, and metastasis (3). Tumor-induced angiogenesis is believed to occur when a small avascular tumor exceeds some critical diameter (~ 2 mm), above which normal tissue vasculature is no longer able to support its growth (4). At this stage, the tumor cells lacking nutrients and oxygen become hypoxic. This is assumed to trigger cellular release of tumor angiogenic factors (TAFs) (5), which start to diffuse into the surrounding tissue and approach the endothelial cells of nearby blood vessels. Endothelial cells subsequently respond to the TAF concentration gradient by forming sprouts, migrating, and proliferating toward the tumor (6, 7). It takes approximately 10 to 21 days for the growing network to link the tumor to the parent vessel (6, 8, 9), and this vascular connection subsequently provides all the nutrients and oxygen required for continued tumor growth. An excellent summary of all the key cell-biological processes involved in angiogenesis can be found in the comprehensive review article of Paweletz & Knierim (10). More recent summaries of specific selected components of angiogenesis can be found in other papers (11–17).

Interest in the mathematical modeling of blood vessel growth and development may be traced back nearly a century to Sir D'Arcy Wentworth Thompson who, in his book *On Growth and Form*, devotes a section entitled "On the Form and Branching of Blood Vessels" and considers "... a number of interesting points in connection with the form and structure of the blood-vessels" (18). The work of Deakin (19) is perhaps the beginning of more recent interest in modeling blood vessel formation, focusing as it does on the migratory response of endothelial cells and capillary loops to angiogenic factors. The modeling is perhaps rather qualitative and heuristic but is interesting in that it attempts to consider the migration of individual endothelial cells in response to TAF. Continuum modeling of angiogenesis using systems of partial differential equations (PDEs) may be considered to start with the work of Balding and McElwain (20) who describe the growth of a capillary network in terms of capillary tip densities and capillary sprout densities in response to TAF.

Over the past 15 years or so, there has been a renewed interest in the mathematical modeling of tumor-induced angiogenesis. The modeling has focused mainly on the key role played by endothelial cells during the formation of the new blood vessels. These models have considered the endothelial cell proliferative and migratory response to different signaling cues arising from the soluble and diffusible angiogenic factors secreted by the cancer cells of the solid tumor and also from signaling cues arising from insoluble molecules (e.g., fibronectin) present in the extracellular matrix. Like the paper of Balding & McElwain (20), the key interactions of the endothelial cells with angiogenic factors and the macromolecules of the matrix have typically led to systems of nonlinear PDEs describing the migration of capillary vessels from the parent vessel across and through the extracellular matrix until they connect with the

solid tumor. However, as with the early model of Deakin (19), some models have a discrete element and have modeled the migration of individual endothelial cells and examined the formation of individual capillary vessels, thus providing insight into the developing capillary network structure.

Key papers in the area include the work of Stokes & Lauffenburger (21), Chaplain & Stuart (22), Byrne & Chaplain (23), Orme & Chaplain (24), Olsen et al. (25), Anderson & Chaplain (26), Chaplain (27), Levine et al. (28), Plank & Sleeman (29). An excellent and comprehensive overview of the mathematical modeling done in this area can be found in the review paper of Mantzaris et al. (30).

By contrast, blood flow modeling in a tumor-induced (micro) capillary network has only been considered relatively recently. Blood is a complex fluid, the rheological properties of which lead to interesting feedback mechanisms during perfusion. For example, shear stresses generated within the capillary network by the flowing blood strongly influence vessel adaptation and network remodeling (31–35). These shear stresses are, in turn, affected by blood viscosity, the distribution of which depends on a nonuniform distribution of hematocrit (volume fraction of red blood cells contained in the blood) within the host vasculature (the Fåhræus effect). However, the distribution of hematocrit depends on the spatial architecture of the underlying network and so the feedback is established, “the modeling loop is closed,” so to speak. Blood rheology and its influence on the remodeling of microvascular networks have been intensely studied by Pries et al. (36–38), both experimentally and theoretically. From these studies Pries and coworkers have formulated a model for vascular adaptation incorporating a number of feedback mechanisms. They have demonstrated that the basic requirement for the generation of stable vascular structures involves a combination of hemodynamic and metabolic stimuli. Mathematical modeling of flow in capillary networks has been undertaken in papers by McDougall et al. (39), Alarcon et al. (40), and Stéphanou et al. (41, 42).

Hematocrit: volume fraction of red blood cells contained in the blood

A MODELING FRAMEWORK FOR ADAPTIVE DYNAMIC TUMOR-INDUCED ANGIOGENESIS

Having provided an overview of the key mathematical modeling papers in the area of tumor-induced angiogenesis, the aim of this review is to provide a critical discussion of the current status of the field and to examine recent new work that considers the flow of blood as a non-Newtonian fluid in an adaptive dynamic capillary network, i.e., a capillary network that evolves both spatially and temporally in response to its associated flow distribution. To achieve this, in the next section we begin with a description of a mathematical model for the growth of a hollow capillary network in the absence of flow. The model is based on that of Anderson & Chaplain (26). Because there is no flow or vessel remodeling, this model may perhaps be considered more appropriate at describing *in vitro* endothelial cell migration and capillary sprout formation. In subsequent sections, we describe how to incorporate flow and show that the impact of this dynamic remodeling and shear-induced vessel branching on the global network architecture is highly significant. Finally, a number of key physical and

Chemotaxis: directed migratory response of cells to soluble, diffusible growth factors

Haptotaxis: directed migratory response of cells to insoluble, nondiffusible molecules

FN: fibronectin

MDE: matrix degrading enzyme

biochemical parameters are varied in the model to assess their effect on the network architecture and to quantify the efficiency of these different networks in carrying blood-borne material to the solid tumor. In doing so, insights are offered into the evolution of chemotherapeutic and antiangiogenic agents during treatment of cancer. This computational approach may provide a rational biomechanical basis for an effect which has been known for over 30 years, namely drug-induced normalization of tumor blood vessels (43, 44). The paper concludes with a discussion section summarizing all the main results and offering directions for future model development and study.

Discrete Modeling of Endothelial Cell Migration and Hollow Capillary Sprout Formation

The model of endothelial cell migration in this section describes how capillary sprouts emerging from a parent vessel migrate toward a tumor, leading to the formation of a vascular network that supplies nutrients for continued development. The model is inspired by the tumor-induced angiogenesis model initially proposed by Anderson & Chaplain (26). The model assumes that endothelial cells migrate through (a) random motility, (b) chemotaxis in response to TAF released by the tumor, and (c) haptotaxis in response to fibronectin (FN) gradients in the extracellular matrix. If we denote by n the endothelial cell density per unit area, then the equation describing endothelial cell conservation is given by

$$\frac{\partial n}{\partial t} = \overbrace{D\nabla^2 n}^{\text{random}} - \overbrace{\nabla \cdot (\chi(c)n\nabla c)}^{\text{chemotaxis}} - \overbrace{\rho\nabla \cdot (n\nabla f)}^{\text{haptotaxis}}. \quad (1)$$

The chemotactic migration is characterized by the function $\chi(c) = \chi/(1 + \delta c)$, which reflects the decrease in chemotactic sensitivity with increased TAF concentration. The coefficients D , χ , and ρ characterize the random, chemotactic, and haptotactic cell migration, respectively.

TAF and the extracellular matrix-macromolecule FN bind to specific membrane receptors on endothelial cells and subsequently trigger molecular cascades inside the ECs, activating cell migratory machinery. One consequence of this activation process is the cells production of matrix degrading enzymes (MDEs), which enhance the attachment of the cells to FN contained in the extracellular matrix. The endothelial cells are consequently able to exert the traction forces required to propel themselves during migration. In the initial model (26), endothelial cell densities and their global influence on TAF and FN concentrations were considered in a continuous formulation. Here, we choose to focus on local effects and consider the influence of each individual cell on its local environment. The model is then given by the following set of equations:

$$\begin{aligned} \frac{\partial c}{\partial t} &= -\eta n_i c, \\ \frac{\partial f}{\partial t} &= \beta n_i - \gamma m f, \\ \frac{\partial m}{\partial t} &= \alpha n_i + \varepsilon \nabla^2 m - \nu m. \end{aligned} \quad (2)$$

Table 1 Vessel branching probabilities according to the local TAF concentration and to the magnitude of the local wall shear stress*

				WSS/ τ_{\max}		
		[0.0,0.2)	[0.2,0.4)	[0.4,0.6)	[0.6,0.8)	[0.8,1.0)
	[0,0,0.3)	0.00	0.00	0.00	0.00	0.00
[TAF]/TAF _{max}	[0.3,0.5)	0.00	0.02	0.04	0.06	0.08
	[0.5,0.7)	0.00	0.03	0.06	0.09	0.12
	[0.7,0.8)	0.00	0.04	0.08	0.12	0.16
	[0.8,1.0)	0.00	0.10	0.20	0.30	0.40

*TAF_{max} is the maximum TAF concentration at $t=0$ and $\tau_{\max}=2$ Pa (20 dynes/cm²), the maximum shear stress derived from preliminary flow simulations.

where c represents the TAF concentration, f the FN concentration, m the MDE concentration, and n_i a Boolean value (1 or 0) that indicates the presence or absence of an endothelial cell at a given position. The parameters β and α characterize the production rate by an individual endothelial cell of FN and MDE, respectively, and η its TAF consumption rate. The major difference with the earlier model is that degradation of fibronectin f , characterized by the coefficient γ , no longer depends directly on the endothelial cell density n . This now depends on the MDE concentration m produced by each individual endothelial cell n_i at rate α (45–47). The MDE, once produced, diffuses locally with diffusion coefficient ε , and is spontaneously degraded at a rate ν .

The displacement of each individual endothelial cell, located at the tips of each growing sprout, is given by the discretized form of the endothelial cell mass conservation equation (Equation 1). The migration of each cell is consequently determined by a set of coefficients emerging from this equation, which relate to the likelihood of the cell remaining stationary, moving left, right, up, or down. These coefficients incorporate the effects of random, chemotactic, and haptotactic movement and depend on the local chemical environment (FN and TAF concentrations). Proliferation of the endothelial cells at the capillary tips and branching at capillary tips are implemented in the model at the discrete level. Tip branching depends on the TAF concentration at a given spatial location (see **Table 1** below). Using the above model, it is possible to generate “hollow” capillary networks that are structurally similar to those observed experimentally (26, 29).

Modeling Blood Flow in the Developing Capillary Network

In this section, we describe how modeling the flow of blood through a growing capillary network can be achieved. At this point, it is worth recalling the prescient words of D’Arcy Thompson on this matter:

“Many problems of a hydrodynamical kind arise in connection with the flow of blood through the blood-vessels; and while these are of primary importance to the physiologist they interest the morphologist in so far as they bear on the questions of structure and

form. As an example of such mechanical problems we may take the conditions which go to determine the manner of branching of an artery, or the angle at which its branches are given off. . . This is a vastly important theme . . . and helps to bring the morphological and the physiological concepts together” (18).

To achieve this, two key modeling assumptions are required, and once again we recall the words of D’Arcy Thompson:

“We rely once more on Poiseuille’s Law . . . but we have also to account for the blood itself” (18).

Blood is a very complex biphasic medium, composed of many different constituents, including red blood cells (erythrocytes), white blood cells (leukocytes), and platelets involved in clotting cascades. These solid elements represent approximately 45% of the total blood composition—red cells are predominant—and are carried in the plasma, which constitutes the fluid phase. A measure of the solid phase is given by the blood hematocrit, which represents the volume fraction of red blood cells contained in the blood. The average human hematocrit has a value of approximately 45%.

Because of its biphasic nature, blood does not behave as a continuum and the viscosity measured while flowing at different rates in microvessels is not constant. Moreover, direct measurement of blood viscosity in living microvessels is very difficult to achieve with any degree of accuracy. Pries et al. (48) have proposed an alternative approach that entails comparisons of the flow distribution in a numerical network (generated by a mathematical model) with similar experimental systems. The relationship that was found to offer the best fit with the experimental data at the microvascular scale is given by

$$\mu_{rel}(R, H_D) = \left[1 + (\mu_{0.45} - 1)f(H_D) \left(\frac{2R}{2R - 1.1} \right)^2 \right] \left(\frac{2R}{2R - 1.1} \right)^2, \quad (3)$$

where $\mu_{0.45}$ is the viscosity corresponding to the normal average value of the discharge hematocrit ($H_D = 0.45$), R the vessel radius, and $f(H_D)$ a function of the hematocrit. These terms are defined as

$$\begin{aligned} \mu_{0.45} &= 6e^{-0.17R} + 3.2 - 2.44e^{-0.06(2R)^{0.0645}}, \\ f(H_D) &= \frac{(1 - H_D)^C - 1}{(1 - 0.45)^C - 1} \\ C &= (0.8 + e^{-0.15R}) \left(-1 + \frac{1}{1 + 10^{-11}(2R)^{12}} \right) + \left(\frac{1}{1 + 10^{-11}(2R)^{12}} \right) \end{aligned} \quad (4)$$

Plots of Equation 3 show that the apparent blood viscosity generally increases with decreasing capillary radius, although the precise relationship is nonlinear since it is actually hematocrit-dependent. The rheological properties of blood defined by equations (3) and (4) have been used in the flow modeling simulations, the results of which are given below.

To calculate flow within the entire interconnected network of capillaries, it is first necessary to decide on a local relationship between the pressure gradient ΔP and flow Q at the scale of a single capillary element of length L and radius R . Such a relationship in the case of a non-Newtonian fluid can be approximated by the following Poiseuille-like expression:

$$Q = \frac{\pi R^4 \Delta P}{8\mu_{app}(R, H_D)L}, \quad (5)$$

where $\mu_{app}(R, H_D) = \mu_{rel} \cdot \mu_{plasma}$ is the product of relative and plasma viscosities. The apparent blood viscosity therefore depends on the local blood hematocrit and radius of the vessel through which the blood is flowing (see Equation 3 above). When considering flow calculations through a network of interconnected capillary elements having distributed radii, one simply conserves mass (or flow if the fluid is incompressible) at each junction where capillary elements meet. Hence, for each node the following expression can be written as

$$\sum_{k=1}^{k=N} Q_{(i,j),k} = 0, \quad (6)$$

where the index k refers to adjacent nodes and $N = 4$ in a fully connected regular 2-D grid or 6 in 3-D. This procedure leads to a set of linear equations for the nodal pressures (P_i) which can be solved numerically using any of a number of different algorithms. Once nodal pressures are known, Equation 5 can be used to calculate the flow in each capillary element in turn. A fuller discussion of the procedure can be found in Reference 39.

Capillary Vessel Adaptation and Remodeling

Blood rheological properties and microvascular network remodeling are interrelated issues, as blood flow creates stresses on the vascular wall (shear stress, pressure, tensile stress) that lead to adaptation of the vascular diameters via either vasodilatation or constriction. In turn, blood rheology (viscosity, hematocrit, etc.) is affected by the new network architecture—consequently, we should expect adaptive angiogenesis to be a highly dynamic process. We follow the work of Pries et al. (36–38, 48) in incorporating vessel adaptation into our model, which considers a number of stimuli affecting vessel diameter that account for the influence of the wall shear stress (S_{wss}), the intravascular pressure (S_p), and a metabolic mechanism depending on the blood hematocrit (S_m). These stimuli form a basic set of requirements to obtain stable network structures with realistic distributions of vessels diameters and flow velocities. A brief description of each follows.

Wall shear stress. Many studies show that vessels adapt their radius to maintain a constant level of wall shear stress (WSS) (36–38, 49). Hence vessel radius tends to increase with increasing WSS, whereas WSS decreases with increasing radius. The WSS stimulus can be described by a logarithmic law as

$$S_{wss} = \log(\tau_w + \tau_{ref}), \quad (7)$$

WSS: wall shear stress

where τ_w is the actual WSS in a vessel segment calculated from

$$\tau_w = \frac{4\mu(R, H_D)}{\pi R^3} |Q|, \quad (8)$$

and τ_{ref} is a constant included to avoid singular behavior at low shear rates (37). Stresses in References 7 and 8 are in dynes/cm². The WSS calculated in the parent vessel of our computational model is of the order 4 Pa (40 dynes/cm²) and capillary values are less than 2 Pa (20 dynes/cm²), in agreement with those measured experimentally in the dog by Kamiya et al. (50). Adaptation in response to the WSS stimulus alone tends to reinforce a single path in the network composed of a few well-established, fully dilated vessels—corresponding to the main flowing backbone of the vasculature—while simultaneously eliminating the low-flow paths. However, the resulting network is unstable in the sense that there is no consistent balance for the radius and flow distribution achieved when S_{wss} is considered in isolation.

Intravascular pressure. Intravascular pressure is another key stimulus for vascular adaptation. Pries et al. (49) have experimentally observed on the rat mesentery the dependence of the magnitude of the WSS with the local intravascular pressure (P). They proposed a parametric description of their experimental data, which exhibits a sigmoidal increase of the wall shear stress with increasing pressure through the following:

$$\tau_c(P) = 100 - 86 \cdot \exp\{-5000 \cdot [\log(\log P)]^{5.4}\}. \quad (9)$$

Pressure is measured in millimeters of mercury (1 mm Hg = 133 Pa) and stresses are again given in dynes per square centimeter. The sensitivity of the corresponding stimulus to intravascular pressure is then described by

$$S_p = -k_p \log \tau_c(P), \quad (10)$$

where k_p is a constant that dictates the relative intensity of the stimulus.

Metabolic hematocrit-related stimulus. The metabolic stimulus effectively stabilizes the adapting network by stimulating vessel growth in areas of the vascular bed exhibiting low flow. The stimulus is once again described by a logarithmic law given by

$$S_m = k_m \log \left(\frac{Q_{ref}}{QH_D} + 1 \right), \quad (11)$$

where Q_{ref} is a reference flow. In our simulations, Q_{ref} corresponds to the flow in the parent vessel. H_D represents the discharge hematocrit in the vessels, Q the flow in the vessel under consideration, and k_m is a constant characterizing the relative intensity of the metabolic stimulus.

Our theoretical model for vessel adaptation assumes that the change in a flowing vessel radius (ΔR) over a time step Δt is proportional to both the global stimulus acting on the vessel and to the initial vessel radius R , i.e.,

$$\Delta R = S_{tot} R \Delta t = (S_{wss} + S_p + S_m) R \Delta t. \quad (12)$$

With the relationships described above, the model for vessel adaptation becomes

$$\Delta R = \left[\underbrace{\log(\tau_w + \tau_{ref})}_{S_{wss}} - \underbrace{k_p \log \tau_e(P)}_{S_p} + \underbrace{k_m \log\left(\frac{Q_{ref}}{QH_D} + 1\right)}_{S_m} - k_s \right] R \Delta t. \quad (13)$$

DATIA: dynamic adaptive tumor-induced angiogenesis

The additional term k_s represents the shrinking tendency of a vessel. This term is interpreted by Pries et al. (36) as reflecting a natural reaction of the basal lamina, which acts to counter any increase in vessel diameter.

Inclusion of the above mechanisms into our modeling framework now allows us to simulate dynamic remodeling of a flowing vasculature. This significant improvement in angiogenesis modeling allows us to describe vascular growth in a far more realistic manner, with areas of the capillary network dilating and constricting in response to variations in perfusion-related stresses and stimuli. The final step in the development of the complete dynamic adaptive tumor-induced angiogenesis (DATIA) model is to couple the network flow modeling approach outlined in this section to the hollow capillary model derived from the endothelial cell migration equations described earlier. This is achieved through the role of wall shear stress.

WSS is known to play a leading role in the growth and branching of capillary vessel networks (37, 38). To “bring the morphological and the physiological concepts together” (18), the cell migration and flow models are coupled by incorporating the mechanism of shear-dependent vessel branching in addition to sprout branching via local TAF concentrations. This allows us to produce capillary network structures that adapt dynamically through adjuvant vessel branching in areas of the network experiencing increased shear stresses following anastomosis elsewhere in the system. We note that because the shear stress is due to the blood flowing through the capillaries, and vessel branching can only occur after some degree of anastomosis has taken place—hence, the early stages of angiogenesis are characterized by vessel branching, which depends only on the TAF concentration.

The combined effects of the local WSS and TAF concentration upon vessel branching probability have been implemented in the model as described in **Table 1**. In the absence of quantitative experimental data, the probabilities chosen for the vessel branching process have been defined on a qualitative basis and reflect the combined influence of the WSS and local TAF concentration. High values of WSS in tandem with high local TAF concentrations lead to a higher branching probability, whereas lower values of one or both of WSS and TAF concentration lead to lower branching probability. For each range of WSS (linearly distributed in [0,1]), the corresponding TAF probability profile has been obtained via a linear scaling of the values reported in McDougall et al. (39) and Stéphanou et al. (41, 42). Note that in the absence of WSS, TAF-dependent sprout tip branching is the only means by which a migrating vessel can bifurcate.

To summarize, the conditions for vessel branching in the DATIA model are as follows: (a) the likelihood of a vessel branching increases with both the local TAF

concentration and the magnitude of the shear stress affecting the vessel wall; and (b) the vessel must reach a certain level of maturation before it is able to branch, although branching cannot occur once a basal lamina has formed around a vessel (51, 52).

One additional constraint on vessel branching is the age of the vessel itself. The time interval within which a vessel can branch has been fixed at 4–8 days in the simulations (i.e., from $\tilde{\tau} = 2.66$ to $\tilde{\tau} = 5.33$). In this interval, the vessel is sufficiently mature for branching to occur yet young enough to ensure that no basal lamina has had time to form, which would contribute considerably to the stabilization of the network (cf. 52, 53).

Model Parameterization and Simulation Details

The domain considered for the computational simulation studies is a square of length $L = 2$ mm and the parent vessel from which the vascular network grows is located at the upper edge of the domain (all subsequent figures). The tumor surface is located along the lower domain boundary (all subsequent figures). We assume that the capillary sprouts and TAF remain confined within the domain and so no-flux boundary conditions are imposed on the boundaries. Initial TAF and fibronectin profiles are the same as those used in McDougall et al. (2002) and vascular growth is initialized by distributing five sprouts at regular intervals along the parent vessel.

Unless otherwise indicated, the dimensionless parameter values used for the simulations presented in this paper were as follows (cf. 26, 39, 41, 42):

$$D = 0.0003, \quad \delta = 0.6, \quad \chi = 0.38, \quad \rho = 0.28$$

$$\eta = 0.1, \quad \beta = 0.05, \quad \gamma = 0.1, \quad \alpha = 10e - 6, \quad \varepsilon = 0.01, \quad \nu = 3$$

The time was scaled as

$$\tilde{t} = \frac{t}{\tau},$$

with $\tau = L^2/D_c$, where $L = 2$ mm was the length of the domain and $D_c = 3 \times 10^{-7} \text{ cm}^2\text{s}^{-1}$ was taken as the diffusion coefficient for TAF (54). We note that the timescale associated with the capillary growth process is of the order several days, whereas flow through the parent vessel and capillary network occurs over a timescale of a few seconds to a few minutes. To address this issue without compromising computational efficiency, it became necessary to develop a simulation framework that allowed remodeling to occur during the growth phase. An idealized procedure would be as follows: (a) model the growth of the capillary network on a timescale $\tilde{\tau}$, using the endothelial cell migration model; (b) pause the endothelial cell migration model whenever a new anastomosis (loop) forms; (c) switch timescales and flow/remodel the entire capillary network as a result of the modified flow geometry until a new steady state has been reached (this typically takes ~ 100 s); and (d) resume network growth using the cell migration model on the $\tilde{\tau}$ timescale.

However, during the later stages of a simulation, the number of anastomoses (loops) increases considerably and the above procedure becomes impractical from a computational point of view. Consequently, it was decided to flow the network to steady state at regular intervals during the growth process. A sensitivity study showed

Table 2 Typical dimension of blood cells and capillaries (56)

Dimension (μm)	
2	Red blood cell thickness and platelets dimension
2.8	Minimum diameter through which a red cell is able to pass
8	Red blood cell diameter
10	Mean capillary diameter
20	Size of the largest white blood cells

that remodeling at intervals of $\Delta\bar{\tau} = 4.0$ was sufficient to produce vascular networks consistent with those generated from simulations incorporating more frequent adaptation. Returning to the timescale for flow, it should be noted that the time step required when dealing with calculations involving convective transport within a network must be less than or equal to the minimum time required for the least efficient capillary element in the network to empty, i.e., $\Delta t = \text{MIN}(V_{\text{cap}}/Q_{\text{cap}})$, where V_{cap} and Q_{cap} correspond to the volume and flowrate of a capillary element, respectively. This procedure ensures that mass (in this case erythrocyte mass through hematocrit) is conserved during a simulation.

To carry out the flow simulations, a number of important physical and biological parameters need to be estimated.

Vessel properties. The initial radius of each capillary segment was taken to be $6\ \mu\text{m}$ and remodeling of the vessels was permitted within a range, from a minimum radius of $2\ \mu\text{m}$ (essentially eliminating flow; see **Table 2**) to a maximum radius of $12\ \mu\text{m}$ (see **Table 2**). In all simulations, the radius of the parent vessel was kept fixed at $14\ \mu\text{m}$. These values correspond to vessel radii at the capillary level, where the size of the vessels are very close to the size of the red blood cells (55).

Adaptation parameters. The parameters used for the base case adaptation model presented in Equation 13 are taken to be (41, 42)

$$k_s = 0.35 \quad k_p = 0.1 \quad k_m = 0.07$$

$$\tau_{\text{ref}} = 0.103 \quad Q_{\text{ref}} = 1.909\text{e}-11,$$

where Q_{ref} corresponds to the flow in the parent vessel, calculated from Equation 3, with $R = 14\ \mu\text{m}$, $L = 2\ \text{mm}$, and $\Delta P = 1200\ \text{Pa}$ (9 mm Hg) (the pressure drop across the parent vessel). The apparent viscosity μ_{app} is calculated from Equation 5 for each vessel segment and incorporates the effect of discharge hematocrit H_D (which is assumed to remain constant at the inlet of the parent vessel). The plasma viscosity μ_{plasma} is $1.2 \times 10^{-3}\ \text{Pa s}$ and this parameterization gives perfusion velocities in the parent vessel of approximately $3\ \text{mm s}^{-1}$. The chosen parameter values pertaining to remodeling stimuli (i.e., the k_i) yielded stable networks in all cases.

One of the main determinants of the extent of vascular remodeling is the intravascular pressure (P). In the simulations carried out here, we have chosen inlet and outlet pressures to ensure average intravascular pressures of approximately 20 mm of

mercury, in accordance with physiological values at the capillary scale. The effect of varying intravascular pressure is examined in more detail later.

COMPUTATIONAL SIMULATION RESULTS

Capillary Network Architecture in the Absence of Flow

The model for tumor-induced capillary growth described by the system of Equations 1 and 2 was solved numerically on a 100×100 (x, y) square grid. The system of Equation 2 was solved for each grid point at each time step, and the resulting variables c and f were then used to calculate the coefficients appearing in the discretized form of Equation 1. These coefficients then define the preferred migratory direction of each endothelial cell, i.e., the direction of growth of each sprout.

Figures 1 and **2** present the simulation results associated with an initial linear gradient of TAF—**Figure 1** shows the network growth and vascular architecture, whereas **Figure 2** shows the associated MDE concentration in the extracellular matrix. We observe in **Figure 1** the stochastic nature of each of the five sprout trajectories as they progress toward the tumor (the surface of which occupies the lower boundary of the domain). Initially, the MDE concentrations are highly localized around

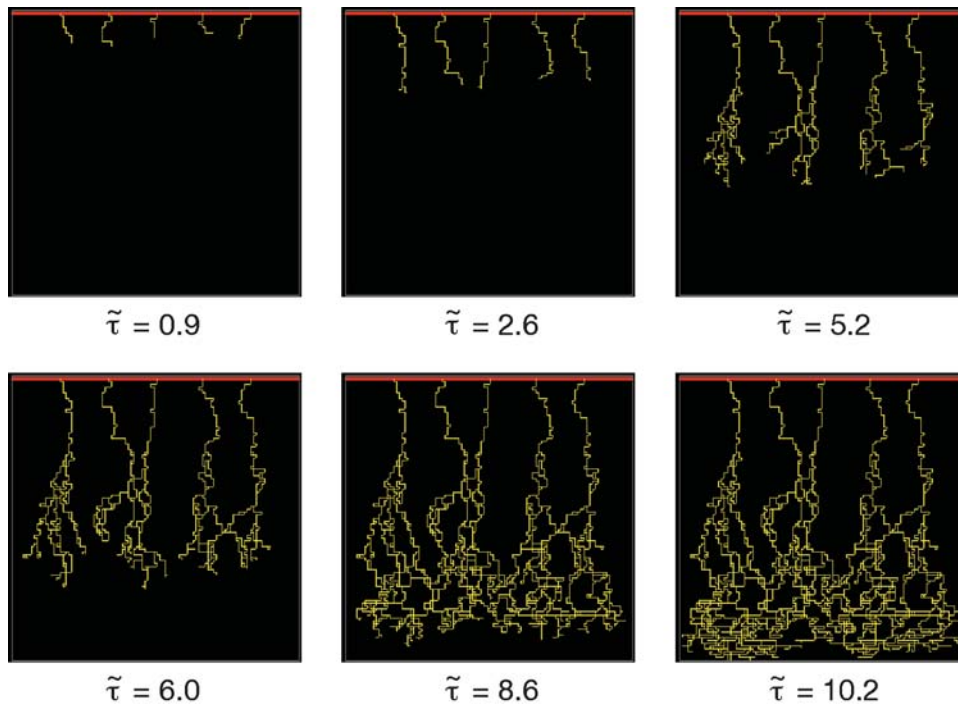


Figure 1

Snapshots of a developing hollow capillary network.

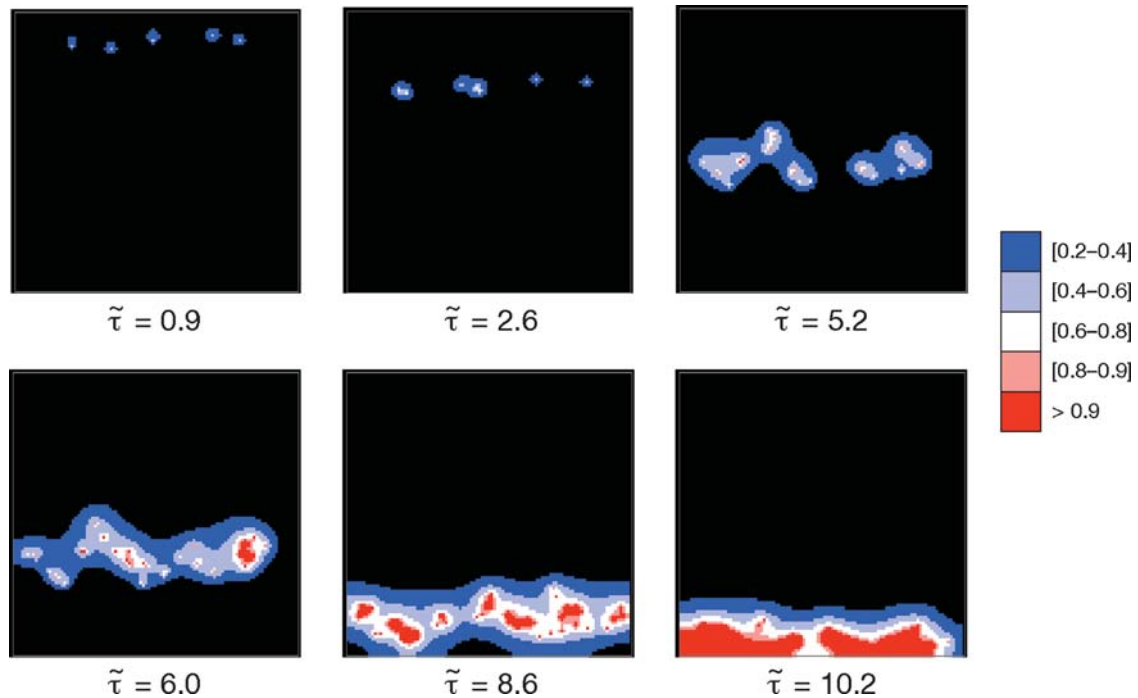


Figure 2

MDE concentration in the extracellular matrix associated with the capillary network shown in **Figure 1**.

the individual sprout tips and the migratory path taken by each vessel is essentially independent of its neighbors. At time $\tilde{\tau} = 2.6$ (corresponding to $t = 3.9$ days), vessels 2 and 3 (numbered from left to right) begin to converge, and by $\tilde{\tau} = 5.2$ (7.8 days) some degree of sprout branching and local anastomosis has already taken place for all five sprouts. Vessels 2 and 3 have now formed an anastomosis (loop), hence perfusion could be expected to occur within the developing capillary bed at this time.

Anastomosis increases considerably with increased sprout branching in regions distal to the parent vessel and the individual vascular trees rapidly connect with one another after $\tilde{\tau} = 6$ (9 days). Regions of high MDE concentration subsequently emerge as the number of migrating, productive tip cells rises, and it becomes clear that the increase in anastomosis is related to an increase in lateral migration owing to the appearance of a connected MDE front as shown in **Figure 2** (from $\tilde{\tau} = 6$). It takes approximately 10 days for the growth process to be completed, i.e., for the vasculature to connect the tumor to the parent vessel and hence to the blood supply.

The structure of the vascular architectures produced by the model at this stage are in good visual agreement with experimental data (8, 9), but the resulting vascular

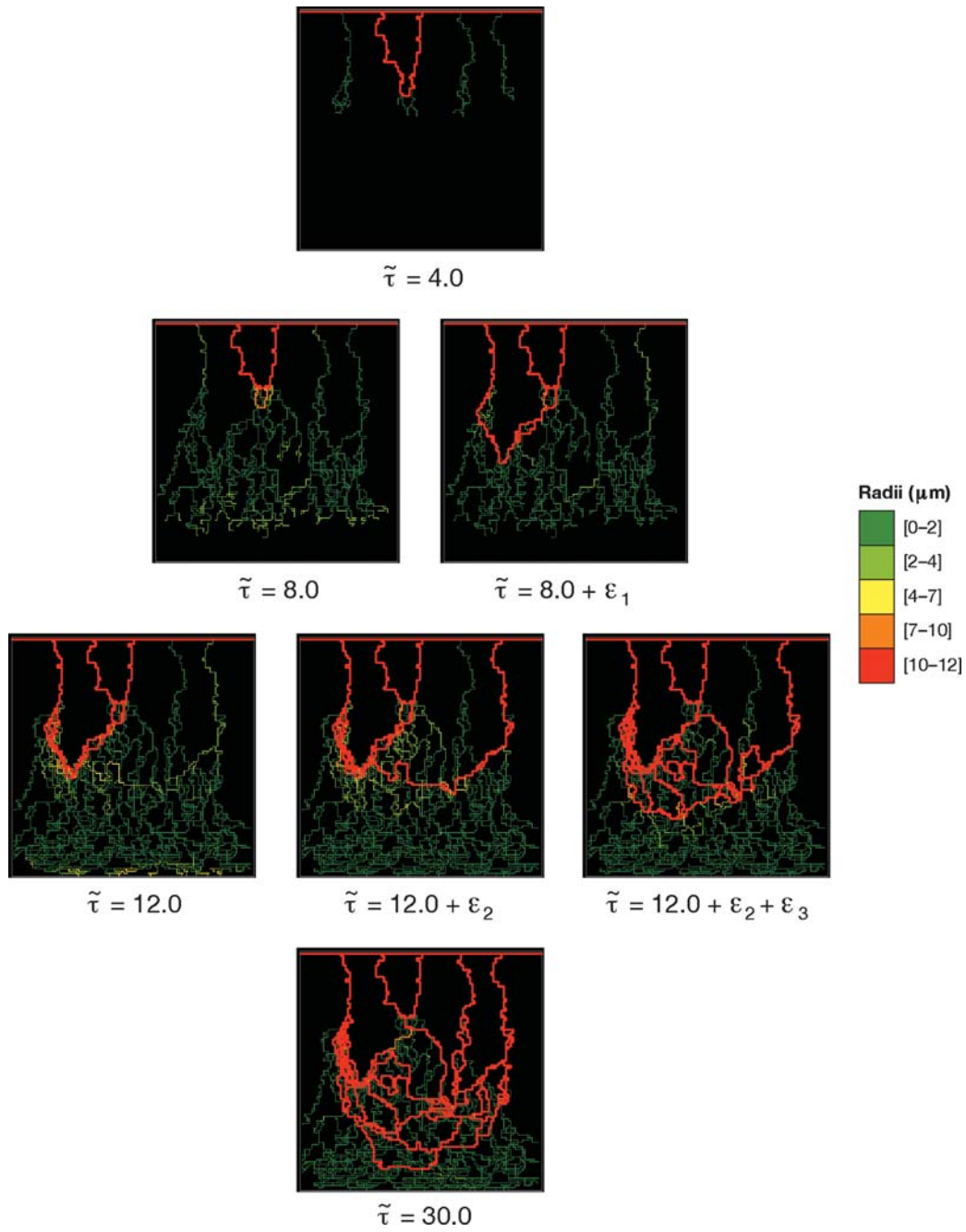


Figure 3

Evolution of capillary network with full DATIA, including wall shear stress-induced branching.

networks lack any variation in capillary radius (a vital factor when considering treatment efficacy). Moreover, vessel branching at this stage only depends on the local TAF concentration and is unaffected by perfusion. In the following section we address this issue through the inclusion of WSS-induced vessel branching.

Dynamic Adaptive Tumor-Induced Angiogenesis

In the simulation results of the previous section, only capillary sprout tip branching was considered. The series of simulations reported in this section in **Figure 3**, however, includes both sprout tip branching and vessel branching under the combined effects of both local TAF concentration and additionally local WSS. Note that sprout tip branching is still important in the production of the first connections between the growing vascular trees, allowing blood to flow into the evolving capillary bed and creating the shear stresses required for the additional vessel branching.

After $\bar{\tau} = 4.0$, additional shear-induced branches emerge from the apex of the loop formed by the anastomosis of vessels 2 and 3. These branches continue to migrate toward the tumor ($\bar{\tau} = 8.0$) and modify the distribution of flow and WSS at subsequent times. Further shear-induced branching is evident in the snapshots at $\bar{\tau} = 12.0$ (18 days), largely associated with the dilated arcade between vessels 1 and 2. The

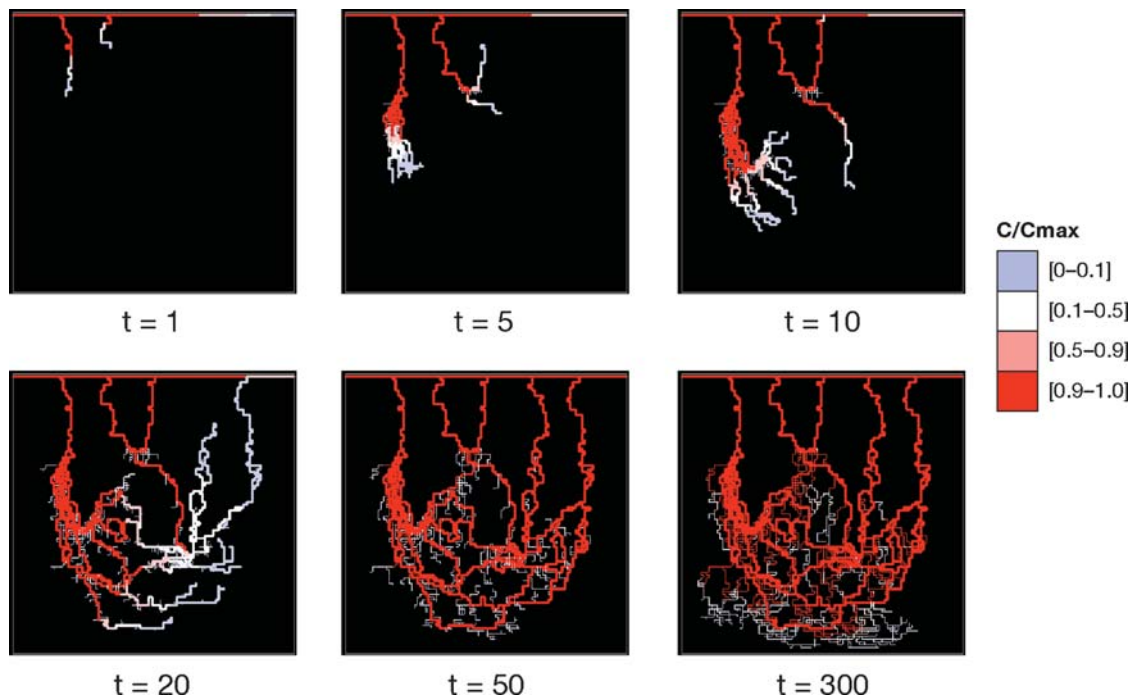


Figure 4

Tracer (drug) concentration distribution in network at different times.

network is essentially at steady state at this stage, with only a small amount of vessel branching occurring after this time.

Probably the most important aspect of this simulation is that it demonstrates how shear-induced branching leads to earlier formation of dilated anastomoses close to the parent vessel. This dilation is positively reinforcing, with proximally dilated loops undergoing further vessel branching. Subsequent migration of these additional branches results in high capillary densities, and the main consequence of this is that the number of dilated, high-conductivity pathways close to the tumor surface is greatly reduced. The impact of these changes in network architecture upon treatment delivery will be discussed in the following section.

TRANSPORT THROUGH ADAPTED NETWORKS: IMPLICATIONS FOR NUTRIENT SUPPLY AND DRUG DELIVERY TO SOLID TUMORS

The main aim of the work presented in this section is to quantify the efficiency of different networks in carrying blood-borne material, e.g., nutrients, chemotherapy drugs, to the tumor. In doing so, it is hoped that some insights can be offered into the precise fate of chemotherapeutic agents in the vasculature during treatment, which could lead to the identification of a number of new therapeutic targets and strategies

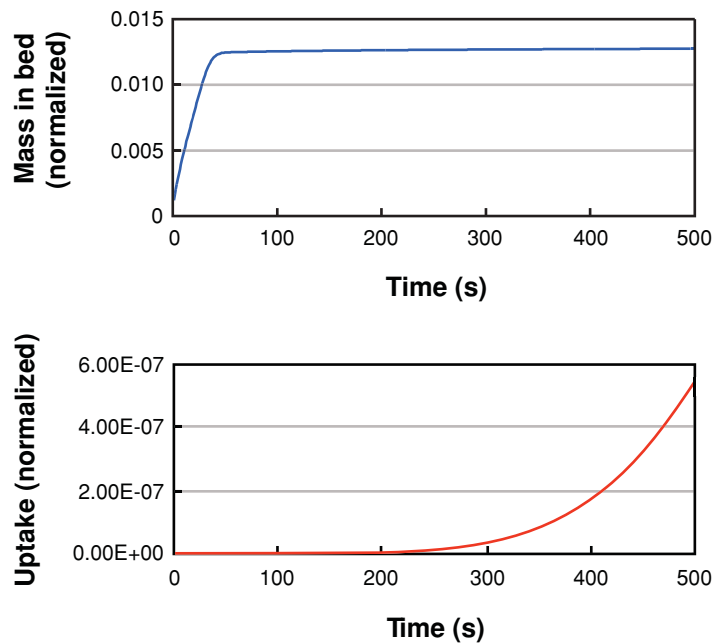


Figure 5

Plots of total drug mass in parent vessel and network over time (*above*) and amount of drug reaching the tumor (*below*).

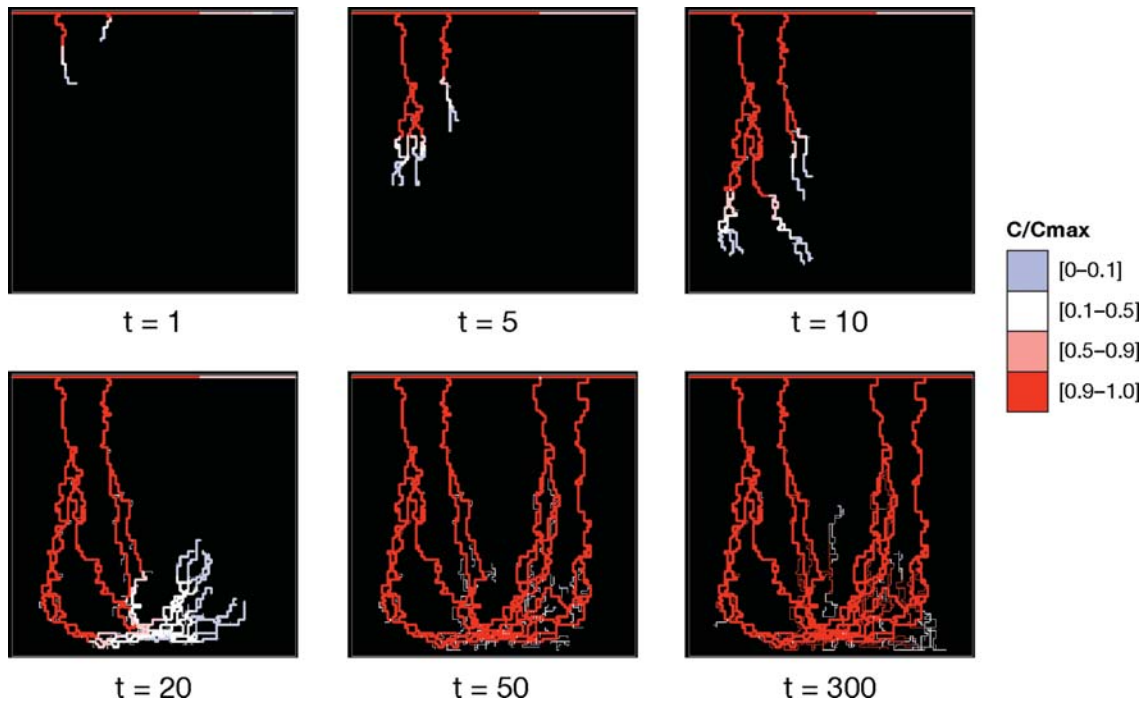


Figure 6

Tracer distribution within network of reduced haptotaxis coefficient.

for tumor management. This approach through the current dynamic adaptive model for tumor-induced angiogenesis provides a rational biomechanical basis to investigate an effect that was first reported over 30 years ago—that of drug-induced normalization of tumor blood vessels—and which has recently been the subject of renewed interest (43, 44, 57–60).

To assess transport efficacy within a given adapted vessel network, a “tracer” at concentration C_{\max} was continuously infused into the inlet of the parent vessel for 500 s. At each time step, the total amount of drug flowing into each capillary junction (node) was calculated, perfect mixing was assumed at each node in the network, and new drug concentrations were calculated for all outflow bonds based on the updated nodal values.

The base-case simulation for transport utilized the vasculature shown in **Figure 3**, i.e., a fully adaptive network that includes shear-induced branching. **Figure 4** shows the tracer evolution through the bed at a number of different times (in seconds). It is immediately clear that the bulk (in fact, almost all) of the injected tracer flows through the highly conductive dilated backbone, largely bypassing the tumor and recirculating to the parent vessel. In excess of 300 s of continuous infusion is required before any tracer reaches the tumor surface, and only then in very small concentrations.

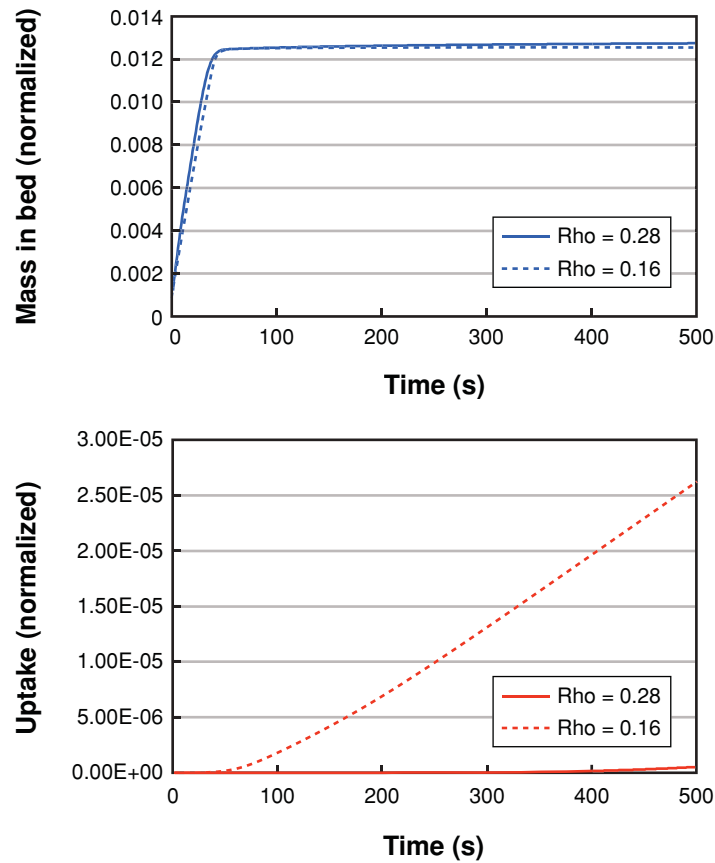


Figure 7

Plots of total drug mass in parent vessel and network over time (*above*) and amount of drug reaching the tumor (*below*). Two different haptotaxis coefficients.

Figure 5 shows plots of the total drug mass in the system (parent vessel and capillary network) and uptake by the tumor as functions of time. It should be noted that (*a*) tumor uptake is considered to be instantaneous once tracer reaches the lower boundary of the domain, and (*b*) all masses have been normalized to the total mass injected into the parent vessel over the course of the simulation. Only approximately 1.5% of the infused tracer even enters the capillary network, and although the total mass in the network reaches a plateau after approximately 50 s (transport being essentially governed by steady-state flow through the dilated backbone), it takes another 200–250 s before uptake commences. This is because capillaries forming part of the brush border close to the tumor surface are narrow and poorly perfused—consequently, only a very small fraction of the injected treatment actually reaches the target. As an aside, it should be noted that, although convective transport would be a rather poor delivery mechanism for large molecules (i.e., cytotoxic treatments), the dilated

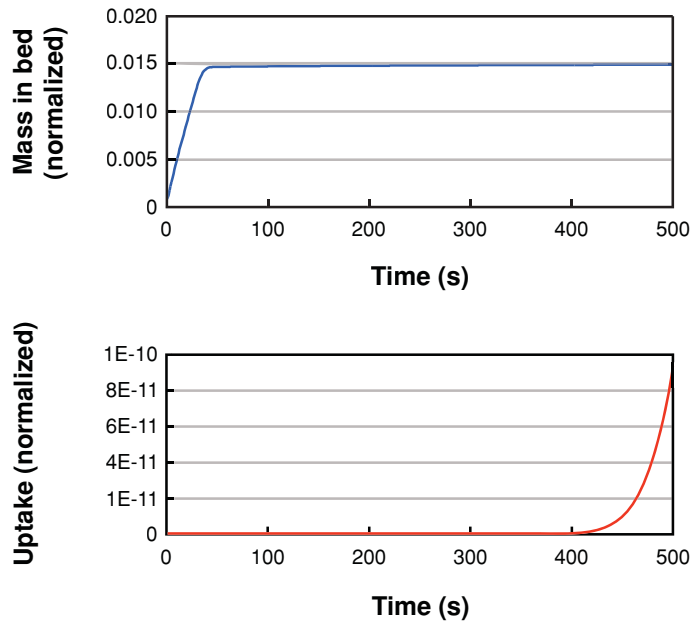


Figure 8

Plots of total drug mass in parent vessel and network over time (*above*) and amount of drug reaching the tumor (*below*). Reduced hematocrit.

network is sufficiently well developed within a few hundred microns of the tumor surface that diffusion of nutrients (oxygen, glucose) would be relatively efficient over the timescale of tumor growth.

Results from a wide range of sensitivity studies using the DATIA model have highlighted a number of new possibilities for therapeutic intervention (61). One possible therapeutic target could be the manipulation of the haptotactic response of the migrating endothelial cells during angiogenesis. A reduction in haptotaxis leads to a capillary network characterized by reduced lateral migration and shear-induced branching. The tracer evolution through this vessel network is shown in **Figure 6** and suggests that tumors supplied by this type of vasculature would be well supplied with nutrients and could be expected to grow rapidly. Paradoxically, however, such tumors would also be highly susceptible to infused treatments, with far more cytotoxic agent reaching the tumor than observed in previous cases. This conjecture is supported by the supply and uptake results from the tracer simulation shown in **Figure 7**. Although the total mass of tracer/drug entering the supplying vasculature is almost identical to that observed in the base case simulation [$\rho = 0.28$, **Figure 5** (*above*)], the drug uptake by the tumor is fifty times greater when lateral migration and vessel branching are reduced.

A depressed hematocrit level was also found to have a big impact on drug delivery, and **Figure 8** shows the therapeutic implications of this phenomenon—more

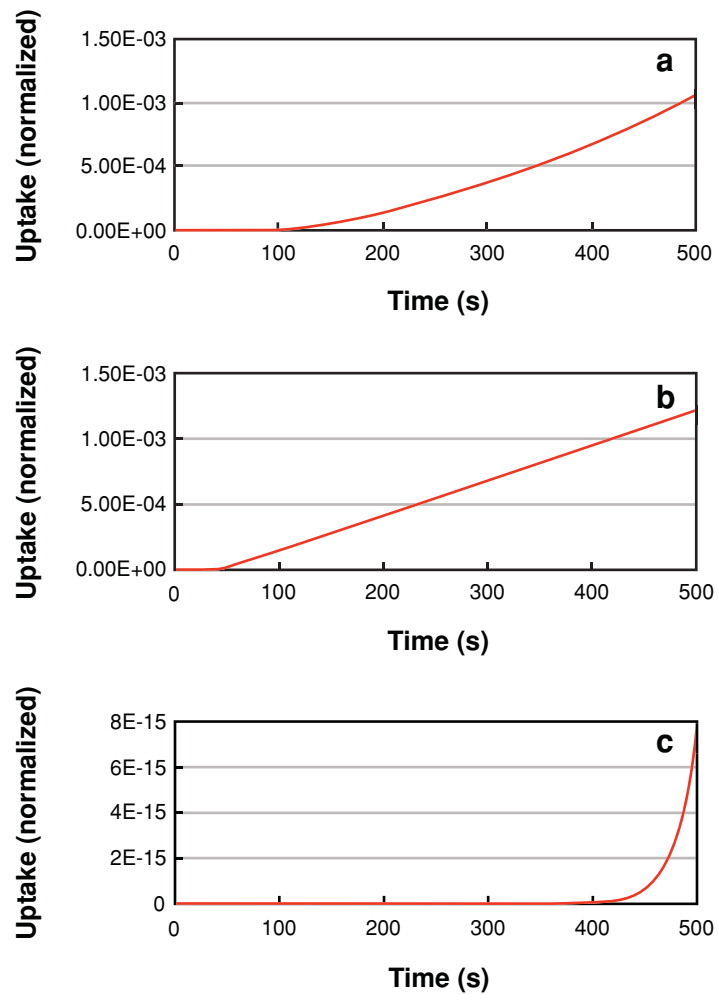


Figure 9

Plots of amount of drug reaching the tumor. (a) Reduced inlet and outlet pressures at parent vessel; (b) lower pressure at inlet parent vessel; (c) increased pressure gradient across parent vessel.

drug enters the capillary network than entered in the base-case simulation, but drug delivery to the tumor is reduced by more than three orders of magnitude.

The overall effect is similar to that observed when the sensitivity of the endothelial cells to shear stress was increased. In the context of nutrient supply to the tumor, it is proposed here that decreasing local hematocrit could be a possible mechanism for generating vasculatures that are detrimental to tumor growth.

The final set of transport simulations presented here relate to networks generated under a variety of intravascular pressure conditions. Note that, in all cases, a pressure

drop of 1200 Pa (9 mm Hg) was applied across the parent vessel when modeling the injection of tracer post angiogenesis. Although pressure conditions used in the development of the network during angiogenesis may have differed from this, maintaining this gradient allows meaningful comparisons to be made across all simulations.

Figure 9a shows uptake for the case when both inlet and outlet parent vessel pressures were reduced by 300 Pa (2.25 mm Hg) prior to angiogenesis. The result, as expected, is in broad agreement with the base case data (**Figure 5b**). This is due to the fact that pressure gradients within the network remain essentially unchanged and so both networks evolve in structurally similar ways. The impact on drug delivery of lowering the pressure at the inlet of the parent vessel by 300 Pa (2.25 mm Hg) prior to angiogenesis, while keeping the outlet pressure unchanged, is shown in **Figure 9b**. Delivery is dramatically increased—by more than three orders of magnitude—and tumors characterized by similar vascular architectures (which exhibit reduced vessel branching owing to reduced wall shear) are consequently highly likely to be vulnerable to chemotherapeutic infusions. The final result concerning the sensitivity of angiogenesis to pressure conditions is that presented in **Figure 9c**. This figure shows the uptake by the tumor supplied by a network where the pressure gradient across the parent vessel was increased by 300 Pa (2.25 mm Hg) prior to angiogenesis. This gives rise to increased, self-reinforcing, vessel branching close to the parent vessel. Uptake is extremely poor, which is not too surprising given the presence of highly dilated loops close to the parent vessel. Hence, intravenous/intraarterial treatments would be expected to prove ineffective in this case.

SUMMARY POINTS

1. Tumor-induced angiogenesis, i.e., the formation of a new network of blood vessels from a preexisting vasculature, is a crucial component of solid tumor growth. The key biological events of this process involve the proliferation and migration of endothelial cells to form new blood vessels, and then subsequent blood flow through these new vessels.
2. Until recently, mathematical modeling of tumor-induced angiogenesis has largely focused on developing models to describe endothelial cell migration and proliferation through the extracellular matrix.
3. Blood rheological properties and the flow of blood through the growing vessels are known to affect the subsequent growth and morphology of the vessels.
4. In this review, we describe a new modeling approach that integrates and explicitly couples a model of endothelial cell migration (26) with a network flow model (39, 41, 42) to evaluate the effects of blood perfusion and radial adaptation on a developing capillary vessel network—a dynamic, adaptive model of capillary growth.

5. The influence of wall shear stress on vessel branching, and, consequently, the major role played by perfusion during capillary growth, has been evaluated, with radial adaptations and vessel remodeling occurring as immediate consequences of primary loop formations (anastomoses).
6. The inclusion of shear-induced capillary branching into the dynamic adaptive model enables the coupling of the flow properties directly to the growing network. This explicit coupling leads to network architectures that differ radically from those found in all previous models.
7. Computational simulations were carried out to investigate the sensitivity of the model to changes in a number of physical and biochemical parameters and how these changes affected the vascular architecture. These included sensitivities to changes in cell-matrix interactions (via the haptotaxis coefficient), blood rheological properties, and intravascular pressure.
8. Initial computational simulations have been undertaken to assess transport efficacy in different vasculatures, and hence nutrient and drug supply to the tumor. These results clearly demonstrated the impact of vessel heterogeneity within a given network on treatment efficacy and highlight the need for incorporating radial adaptations into any angiogenesis model involving transport issues, such as chemotherapeutic intervention.

FUTURE DIRECTIONS

1. A mathematical model of a three-dimensional dynamic, adaptive vasculature is currently being developed.
2. The results from computational simulations of the current two-dimensional mathematical model have suggested a number of important new targets for therapeutic intervention, and these need to be tested experimentally.
3. A fully three-dimensional DATIA model will provide a solid biomechanical basis with which to examine in more detail the possibility of normalizing tumor blood vessels as a means of effectively treating solid tumors (43, 44).

ACKNOWLEDGMENTS

The authors gratefully acknowledge the support of the European Community, through the Marie Curie Research Training Network Project HPRN-CT-2004-503661: Modelling, Mathematical Methods and Computer Simulation of Tumor Growth and Therapy.

LITERATURE CITED

1. Risau W. 1997. Mechanisms of angiogenesis. *Nature* 386:671–74
2. Walsh DA. 1999. Angiogenesis and arthritis. *Rheumatology* 38:103–12
3. Folkman J. 1995. Angiogenesis in cancer, vascular, rheumatoid and other disease. *Nat. Med.* 1:21–31
4. Folkman J. 1971. Tumor angiogenesis: therapeutic implications. *N. Engl. J. Med.* 285:1182–86
5. Folkman J, Klagsbrun M. 1987. Angiogenic factors. *Science* 235:442–47
6. Ausprunk DH, Folkman J. 1977. Migration and proliferation of endothelial cells in preformed and newly formed blood vessels during tumour angiogenesis. *Microvasc. Res.* 14:53–65
7. Sholley MM, Ferguson GP, Seibel HR, Montour JL, Wilson JD. 1984. Mechanisms of neovascularization. Vascular sprouting can occur without proliferation of endothelial cells. *Lab. Invest.* 51:624–34
8. Gimbrone MA, Cotran RS, Leapman SB, Folkman J. 1974. Tumor growth and neovascularization: an experimental model using the rabbit cornea. *J. Natl. Cancer Inst.* 52:413–27
9. Muthukkaruppan VR, Kubai L, Auerbach R. 1982. Tumor-induced neovascularization in the mouse eye. *J. Natl. Cancer Inst.* 69:699–705
10. Paweletz N, Knierim M. 1989. Tumor-related angiogenesis. *Crit. Rev. Oncol. Hematol.* 9:197–242
11. Carmeliet P. 2003. Angiogenesis in health and disease. *Nature Med.* 9:653–60
12. Cleaver O, Melton DA. 2003. Endothelial signaling during development. *Nat. Med.* 9:661–68
13. Ferrara N, Gerber H-P, LeCouter J. 2003. The biology of VEGF and its receptors. *Nat. Med.* 9:669–76
14. Jain RK. 2003. Molecular regulation of vessel maturation. *Nat. Med.* 9:685–93
15. Pugh CW, Ratcliffe PJ. 2003. Regulation of angiogenesis by hypoxia: role of the HIF system. *Nat. Med.* 9:677–84
16. Rafii S, Lyden D. 2003. Therapeutic stem and progenitor cell transplantation for organ vascularization and regeneration. *Nat. Med.* 9:702–12
17. Ylä-Herttuala S, Alitalo K. 2003. Gene transfer as a tool to induce therapeutic vascular growth. *Nat. Med.* 9:694–701
18. Thompson DW. 1917. *On Growth and Form*. Cambridge: Cambridge Univ. Press
19. Deakin AS. 1976. Model for initial vascular patterns in melanoma transplants. *Growth* 40:191–201
20. Balding D, McElwain DLS. 1985. A mathematical model of tumour-induced capillary growth. *J. Theor. Biol.* 114:53–73
21. Stokes CL, Lauffenburger DA. 1991. Analysis of the roles of microvessel endothelial cell random motility and chemotaxis in angiogenesis. *J. Theor. Biol.* 152:377–403
22. Chaplain MAJ, Stuart AM. 1993. A model mechanism for the chemotactic response of endothelial cells to tumour angiogenesis factor. *IMA J. Math. Appl. Med. Biol.* 10:149–68

23. Byrne HM, Chaplain MAJ. 1995. Mathematical models for tumour angiogenesis: numerical simulations and nonlinear wave solutions. *Bull. Math. Biol.* 57:461–86
24. Orme ME, Chaplain MAJ. 1997. Two-dimensional models of tumour angiogenesis and anti-angiogenesis strategies. *IMA J. Math. Appl. Med. Biol.* 14:189–205
25. Olsen L, Sherratt JA, Maini PK, Arnold F. 1997. A mathematical model for the capillary endothelial cell-extracellular matrix interactions in wound-healing angiogenesis. *IMA J. Math. Appl. Med. Biol.* 14:261–81
26. Anderson ARA, Chaplain MAJ. 1998. Continuous and discrete mathematical models of tumor-induced angiogenesis. *Bull. Math. Biol.* 60:857–99
27. Chaplain MAJ. 2000. Mathematical modelling of angiogenesis. *J. Neurooncol.* 50:37–51
28. Levine HA, Pamuk S, Sleeman BD, Nielsen-Hamilton M. 2001. Mathematical modeling of the capillary formation and development in tumor angiogenesis: penetration into the stroma. *Bull. Math. Biol.* 63:801–63
29. Plank MJ, Sleeman BD. 2004. Lattice and non-lattice models of tumour angiogenesis. *Bull. Math. Biol.* 66:1785–819
30. Mantzaris NV, Webb S, Othmer HG. 2004. Mathematical modeling of tumor-induced angiogenesis. *J. Math. Biol.* 49:111–87
31. Lehoux S, Tedgui A. 1998. Signal transduction of mechanical stresses in the vascular wall. *Hypertension* 32:338–45
32. Taber LA. 1998. An optimization principle for vascular radius including the effects of smooth muscle tone. *Biophys. J.* 74:109–14
33. Quick CM, Young WL, Leonard EF, Joshi S, Gao E, et al. 2000. Model of structural and functional adaptation of small conductance vessels to arterial hypotension. *Am. J. Physiol. Heart Circ. Physiol.* 279:H1645–53
34. Godde R, Kurz H. 2001. Structural and biophysical simulation of angiogenesis and vascular remodeling. *Dev. Dyn.* 220:387–401
35. Fisher AB, Chien S, Barakat AI, Nerem RM. 2001. Endothelial cellular response to altered shear stress. *Am. J. Physiol. Lung Cell Mol. Physiol.* 281:L529–33
36. Pries AR, Secomb TW, Gaehtgens P. 1998. Structural adaptation and stability of microvascular networks: theory and simulation. *Am. J. Physiol. Heart Circ. Physiol.* 275(44):H349–60
37. Pries AR, Reglin B, Secomb TW. 2001. Structural adaptation of microvascular networks: functional roles of adaptive responses. *Am. J. Physiol. Heart Circ. Physiol.* 281:H1015–25
38. Pries AR, Reglin B, Secomb TW. 2001. Structural adaptation of vascular networks: role of the pressure response. *Hypertension* 38:1476–79
39. McDougall SR, Anderson ARA, Chaplain MAJ, Sherratt JA. 2002. Mathematical modelling of flow through vascular networks: implications for tumour-induced angiogenesis and chemotherapy strategies. *Bull. Math. Biol.* 64:673–702
40. Alarcon T, Byrne H, Maini P. 2003. A cellular automaton model for tumour growth in inhomogeneous environment. *J. Theor. Biol.* 225:257–74
41. Stéphanou A, McDougall SR, Anderson ARA, Chaplain MAJ. 2005. Mathematical modelling of flow in 2D and 3D vascular networks: applications to anti-angiogenic and chemotherapeutic drug strategies. *Math. Comput. Model.* 41:1137–56

42. Stéphanou A, McDougall SR, Anderson ARA, Chaplain MAJ. 2006. Mathematical modelling of the influence of blood rheological properties upon adaptive tumour-induced angiogenesis. *Math. Comput. Model.* In press
43. Salsbury AJ, Burrage K, Hellmann K. 1970. Inhibition of metastatic spread by ICRF159—selective deletion of a malignant characteristic. *Br. Med. J.* 4:344–46
44. Le Serve AW, Hellmann K. 1972. Metastases and the normalization of tumour blood vessels by ICRF 159: a new type of drug action. *Br. Med. J.* 1:597–601
45. Anderson ARA, Chaplain MAJ, Newman EL, Steele RJC, Thompson AM. 2000. Mathematical modelling of tumour invasion and metastasis. *J. Theor. Med.* 2:129–54
46. Lolas G. 2003. *Mathematical modelling of the urokinase plasminogen activator system and its role in cancer invasion of tissue.* PhD thesis, Univ. Dundee. 303 pp.
47. Anderson ARA. 2005. A hybrid mathematical model of solid tumour invasion: the importance of cell adhesion. *Math. Med. Biol.* 22:163–86
48. Pries AR, Secomb TW, Gaehtgens P. 1996. Biophysical aspects of blood flow in the microvasculature. *Cardiovasc. Res.* 32:654–67
49. Fung YC. 1993. *Biomechanics.* New York: Springer-Verlag
50. Kamiya A, Bukhari R, Togawa T. 1984. Adaptive regulation of wall shear stress optimizing vascular tree function. *Bull. Math. Biol.* 46:127–37
51. Gee MS, Procopio WN, Makonnen S, Feldman MD, Yeilding NM. et al. 2003. Tumor vessel development and maturation impose limits on the effectiveness of anti-vascular therapy. *Am. J. Pathol.* 162:183–93
52. Benjamin LE, Hemo I, Keshet E. 1998. A plasticity window for blood vessel remodelling is defined by pericyte coverage of the preformed endothelial network and is regulated by PDGF- β and VEGF. *Development* 125:1591–98
53. Morikawa S, Baluk P, Kaidoh T, Haskell A, Jain RK, et al. 2002. Abnormalities in pericytes on blood vessels and endothelial sprouts in tumors. *Am. J. Pathol.* 160:985–1000
54. Bray D. 1992. *Cell Movements.* New York: Garland Publ.
55. Ciofalo M, Collins MW, Hennessy TR. 1999. Microhydrodynamics phenomena in the circulation. In *Nanoscale Fluid Dynamics in Physiological Processes. A Review Study*, pp. 219–36. Southampton: WIT Press
56. Secomb TW. 1995. Mechanics of blood flow in the microcirculation. *Symp. Soc. Exp. Biol.* 49:305–21
57. Jain RK. 2001. Normalizing tumor vasculature with anti-angiogenic therapy: a new paradigm for combination therapy. *Nat. Med.* 7:987–89
58. Hellmann K. 2003. Dynamics of tumour angiogenesis: Effect of razoxane-induced growth rate slowdown. *Clin. Exp. Met.* 20:95–102
59. Hellmann K. 2004. Recognition of tumor blood vessel normalization as a new antiangiogenic concept. *Nat. Med.* 10:329
60. Jain RK. 2004. Recognition of tumor blood vessel normalization as a new antiangiogenic concept. *Nat. Med.* 10:329–30
61. McDougall SR, Anderson ARA, Chaplain MAJ. 2006. Mathematical modelling of dynamic adaptive tumour-induced angiogenesis: clinical implications and therapeutic targeting strategies. *J. Theor. Biol.* In press